available at www.sciencedirect.com

ScienceDirect

journal homepage: www.elsevier.com/locate/ijrefrig

# Impact of plate design on the performance of welded type plate heat exchangers for sorption cycles

*Jong Yun Jeong*[a], *Hi ki Hong*[a], *Sun Kuk Kim*[b], *Yong Tae Kang*[a,*,1]

[a]*School of Mechanical and Industrial System Engineering, Kyung Hee University, Yong In, Gyeong-gi 449-701, Republic of korea*
[b]*College of Civil and Architectural Engineering, Kyung Hee University, Yong In, Gyeong-gi 449-701, Republic of Korea*

ARTICLE INFO

*Article history:*
Received 1 November 2008
Received in revised form
12 January 2009
Accepted 15 January 2009
Published online 4 February 2009

*Keywords:*
Heat exchanger
Plate exchanger
Sorption system
Simulation
Computational fluid dynamics
Heat transfer
Pressure drop

ABSTRACT

Numerical and experimental analysis was carried out to examine the heat transfer and pressure drop characteristics of welded type plate heat exchangers for absorption application using Computational Fluid Dynamics (CFD) technique. The simulation results based on CFD are compared with experimental results. A commercial CFD software package (FLUENT) has been used to predict the characteristics of heat transfer, pressure drop and flow distribution within the plate heat exchangers. In this paper, a welded plate heat exchanger with a plate of chevron embossing type was tested by controlling mass flow rate, solution concentration, and inlet/outlet temperatures. The working fluid is $H_2O$/LiBr solution with the LiBr concentration of 54–62% in mass. The numerical simulation examines the internal flow patterns, temperature distribution and the pressure distribution within the channel of the plate heat exchanger. Three plates of embossing types; chevron embossing, elliptic and round, are proposed and simulated in this paper. The simulation results show reasonably good agreement with the experimental results. Also, the numerical results show that the plate with the elliptical shape gives better performance than the plate of the chevron shape from the viewpoints of heat transfer and pressure drop.



# Impact de la conception de la plaque sur la performance des échangeurs de chaleur de type plaques brasées utilisés pour les cycles à sorption

*Mots clés :* Échangeur de chaleur ; Échangeur à plaque ; Système à sorption ; Simulation ; Dynamique numérique des fluides ; Transfert de chaleur ; Chute de pression

* *Corresponding author*. Tel.: +82 31 201 2990; fax: +82 31 202 3260.
E-mail address: ytkang@khu.ac.kr (Y.T. Kang).
[1] IIR B2 session Vice President.
0140-7007/$ – see front matter © 2009 Elsevier Ltd and IIR.
doi:10.1016/j.ijrefrig.2009.01.028

**Nomenclature**

| | |
|---|---|
| $A$ | heat transfer area, $m^2$ |
| $A_c$ | cross section area, $m^2$ |
| $b$ | channel gap distance, m |
| $Cp$ | constant pressure specific heat, $kJ\,kg^{-1}\,K^{-1}$ |
| $D_h$ | hydraulic diameter, m |
| $\Delta T$ | temperature difference, K |
| $F$ | friction factor |
| $G_c$ | channel mass velocity, $kg\,m^{-2}\,s^{-1}$ |
| $\dot{m}$ | mass flow rate, $kg\,s^{-1}$ |
| $L_v$ | vertical length of plate, m |
| $N_t$ | total number of plates |
| $p$ | pressure, kPa |
| $P_n$ | number of passes |
| $Q$ | heat transfer rate, W |
| $t$ | time, s |
| $u$ | velocity, $m\,s^{-1}$ |
| $U$ | overall heat transfer coefficient, $kW\,m^{-1}\,K^{-1}$ |
| $w$ | plate width, m |
| $x$ | coordinate |

*Greek*

| | |
|---|---|
| $\delta$ | Kronecker delta |
| $\varepsilon$ | turbulent kinetic energy |
| $\kappa$ | turbulent kinetic dissipation |
| $\mu$ | viscosity, $kg\,m^{-1}\,s^{-1}$ |
| $\rho$ | density, $kg\,m^{-3}$ |
| $\sigma$ | turbulent Prandtl number |

*Subscripts*

| | |
|---|---|
| $c$ | cold side |
| $FP$ | flow pass |
| $h$ | hot side |
| $i,j,k$ | axis indexes of space coordinates |
| $in$ | inlet |
| $l$ | molecular |
| $m$ | mean |
| $out$ | outlet |
| $p$ | port |
| $t$ | turbulence |
| $'$ | fluctuating quantity |

## 1. Introduction

Due to the environmental problems caused by CFCs and HCFCs such as ozone depletion and global warming by $CO_2$ emission, the development of high efficient absorption refrigeration systems driven by thermal energy has become an important issue. In absorption refrigeration systems, the solution heat exchanger plays an important role in the enhancement of the system performance. Solution recuperative heat exchangers are typically shell and tube or plate heat exchanger.

Recently, a number of studies on high efficient solution heat exchangers have been carried out. Phan et al. (2000) measured heat transfer coefficient and pressure drop in solution heat exchangers for various mass flow rates. Kim et al. (2005) investigated the flow characteristics within brazed type plate heat exchangers (PHE), and quantified the effect of mass flow rate, solution concentration and geometric conditions such as chevron angle on the heat transfer and pressure drop. Galeazzo et al. (2006) studied a virtual prototype of a plate heat exchanger using CFD. Their experimental results were compared to the numerical predictions for heat load obtained from CFD model. The CFD model represented channels, plates and conduits of the heat exchanger and took into account the unequal flow distribution among the channels and the flow mal-distribution inside the channels. The performance of a water–lithium bromide absorption chiller operating with plate heat exchangers was studied by de Vega et al. (2006). A LiBr–water absorption system with brazed type plate heat exchangers for the desorber, the condenser and the solution heat recoverer is considered. Their plate surfaces were grooved with a corrugated sinusoidal shape and 60° chevron angle.

Typically plate heat exchangers are categorized into three types depending on the construction mode; gasket type, brazed type and welded type. In the present study, welded type plate heat exchangers are tested for $H_2O$/LiBr absorption applications.

The objectives of the present study are to develop a welded type PHE with embosses on the plates and to compare the pressure drop and heat transfer characteristics within the embossing plates. Three different embossing plates are compared; chevron, elliptic and round embossing type plates. Numerical results are compared with experimental results. The results from the present study can be used as reference data for real absorption applications of the newly developed plate heat exchanger.

## 2. Modeling for numerical analysis

### 2.1. *Computational fluid dynamics (CFD) modeling*

The simulation of plate heat exchanger is performed by solving the governing equations of mass, momentum and energy conservations using CFD. Figs. 1, 2 and 3 show three different embossing plates simulated in this study; chevron,

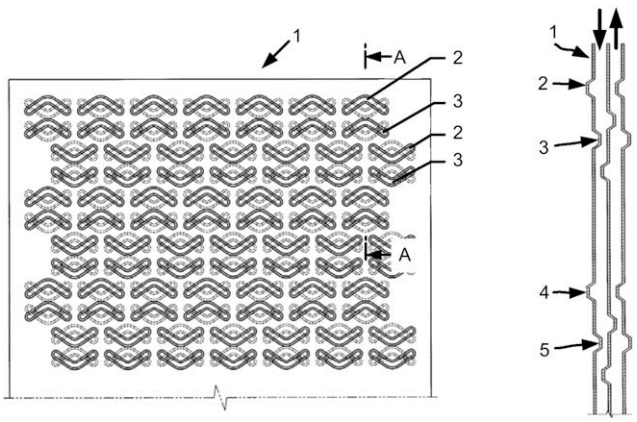


**Fig. 1 – Geometry of chevron embossing type.**

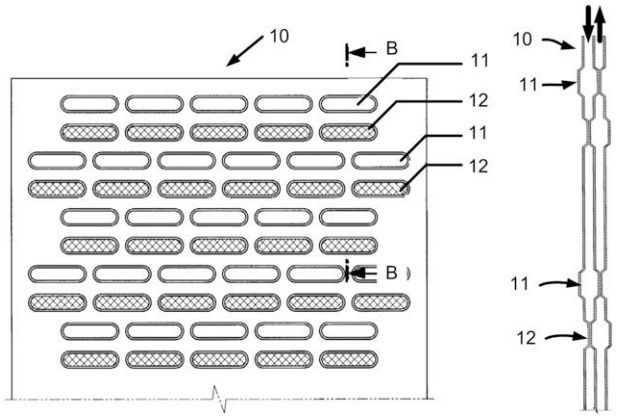


**Fig. 2 – Geometry of elliptic embossing type.**

elliptic and round embossing types, respectively. All plates have same dimensions of 1839 mm in length and 294 mm in width. In FLUENT, the conservation equations of mass, momentum are solved using the finite volume method.

There are several turbulence models available in the code. The turbulence flow is calculated by the SIMPLE method and a first-order upwind difference scheme for the convection–diffusion treatment. To model the heat transfer process between channels in a plate heat exchanger, the following assumptions are made;

(1) The thermo-physical properties of the fluids are constant.
(2) Heat transfer takes place only between the channels and not between the channels and the ports
(3) No heat loss to the surroundings.
(4) Uniform distribution of flow through the channels of a pass.

Since the objectives of this study are to develop various types of embossing plates and to compare the heat transfer and pressure drop characteristics for the plate heat exchanger with the embossing plates, the thermo-physical properties of the solution are calculated based on the average temperatures of the hot and cold solutions in the present study.

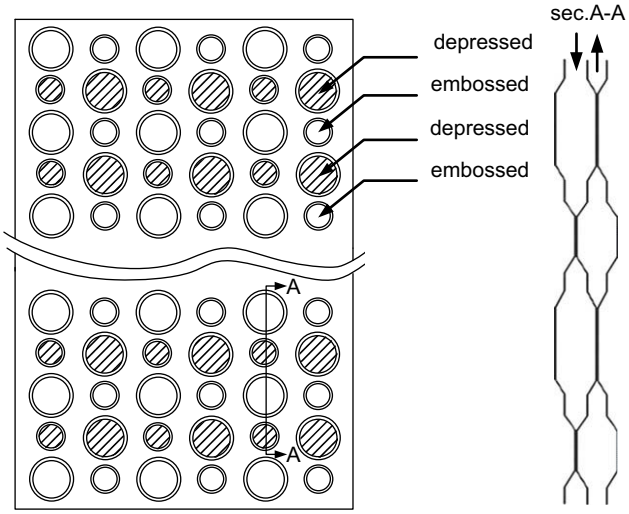


**Fig. 3 – Geometry of round embossing type.**

The governing equations are summarized as follows:

Mass conservation equations:

$$\frac{\partial \rho}{\partial t} + \frac{\partial}{\partial x_i}(\rho u_i) = 0 \tag{1}$$

$$u_i = \overline{u_i} + u_i' \tag{2}$$

where $\overline{u_i}$ and $u_i'$ are the mean and instantaneous fluctuation velocity components, respectively.

$$\frac{\partial}{\partial t}(\rho u_i) + \frac{\partial}{\partial x_i}(\rho u_i u_j) = -\frac{\partial p}{\partial x_i} + \frac{\partial}{\partial x_j}\left[\mu\left(\frac{\partial u_i}{\partial x_j} + \frac{\partial u_j}{\partial x_i} - \frac{2}{3}\partial_{ij}\frac{\partial u_l}{\partial x}\right)\right] + \frac{\partial}{\partial x_j}\left(-\rho\overline{u_i' u_j'}\right) \tag{3}$$

where $\mu$ is the dynamic viscosity of the solution. The standard $\kappa - \varepsilon$ turbulence model has been used and the turbulent kinetic energy and dissipation equations are given as follows (Hinze, 1975);

Turbulent kinetic energy ($\kappa$) equations;

$$\frac{\partial}{\partial t}(\rho k) + \frac{\partial}{\partial x_i}(\rho u_i k) = \frac{\partial}{\partial x_i}\left[\left(\mu + \frac{\mu_t}{\sigma_k}\right)\frac{\partial k}{\partial x_i}\right] + G_k - \rho\varepsilon \tag{4}$$

Turbulent kinetic dissipation ($\varepsilon$) equations;

$$\frac{\partial}{\partial t}(\rho \varepsilon) + \frac{\partial}{\partial x_i}(\rho u_i k) = \frac{\partial}{\partial x_i}\left[\left(\mu + \frac{\mu_t}{\sigma_k}\right)\frac{\partial \varepsilon}{\partial x_i}\right] + C_{1\varepsilon}\frac{\varepsilon}{k}G_k - C_{2\varepsilon}\rho\frac{\varepsilon^2}{k} \tag{5}$$

Turbulent viscosity and model constants;

$$\mu_t = \rho C_\mu \frac{k^2}{\varepsilon} \tag{6}$$

$$G_k = -\rho\overline{u_i' u_j'}\frac{\partial u_i}{\partial x_i} \tag{7}$$

where $C_{1\varepsilon}$, $C_{2\varepsilon}$, and $C_\mu$ are the closure coefficients (Ciofalo et al., 1996).

### 2.2. *Initial and boundary conditions*

The thermal initial and boundary conditions are based on a $H_2O$/LiBr absorption chiller of 210RT which is most widely used in real field. The base mass flow rate of the cold side is 2.0 kg s$^{-1}$, and the inlet temperature of the cold side solution is kept constant 362.0 K. The mass flow rate varies from 1.2 kg s$^{-1}$ to 2.0 kg s$^{-1}$ in the present simulation. No slip and constant heat flux conditions are assumed at the wall. The simulation is carried out based on the cold side, and the thermal conditions for the hot side are given by the heat fluxes. Table 1 summarizes the thermal conditions used in the present study, which are based on the experimental results.

**Table 1 – Thermal conditions**

| | |
|---|---|
| Mass flow rate (kg s$^{-1}$) | 2.0, 1.8, 1.6, 1.4, 1.2 |
| Perimeter, $P_w$ (m) | 0.084 |
| Hydraulic diameter, $D_h$ (m) | 0.00318 |
| Turbulence intensity, $I$ | 0.05 |
| Reynolds Number, $Re_D$ | 118–197 |
| Heat flux (kW m$^{-2}$) | 4.5, 3.96, 3.76, 3.51, 3.0 |

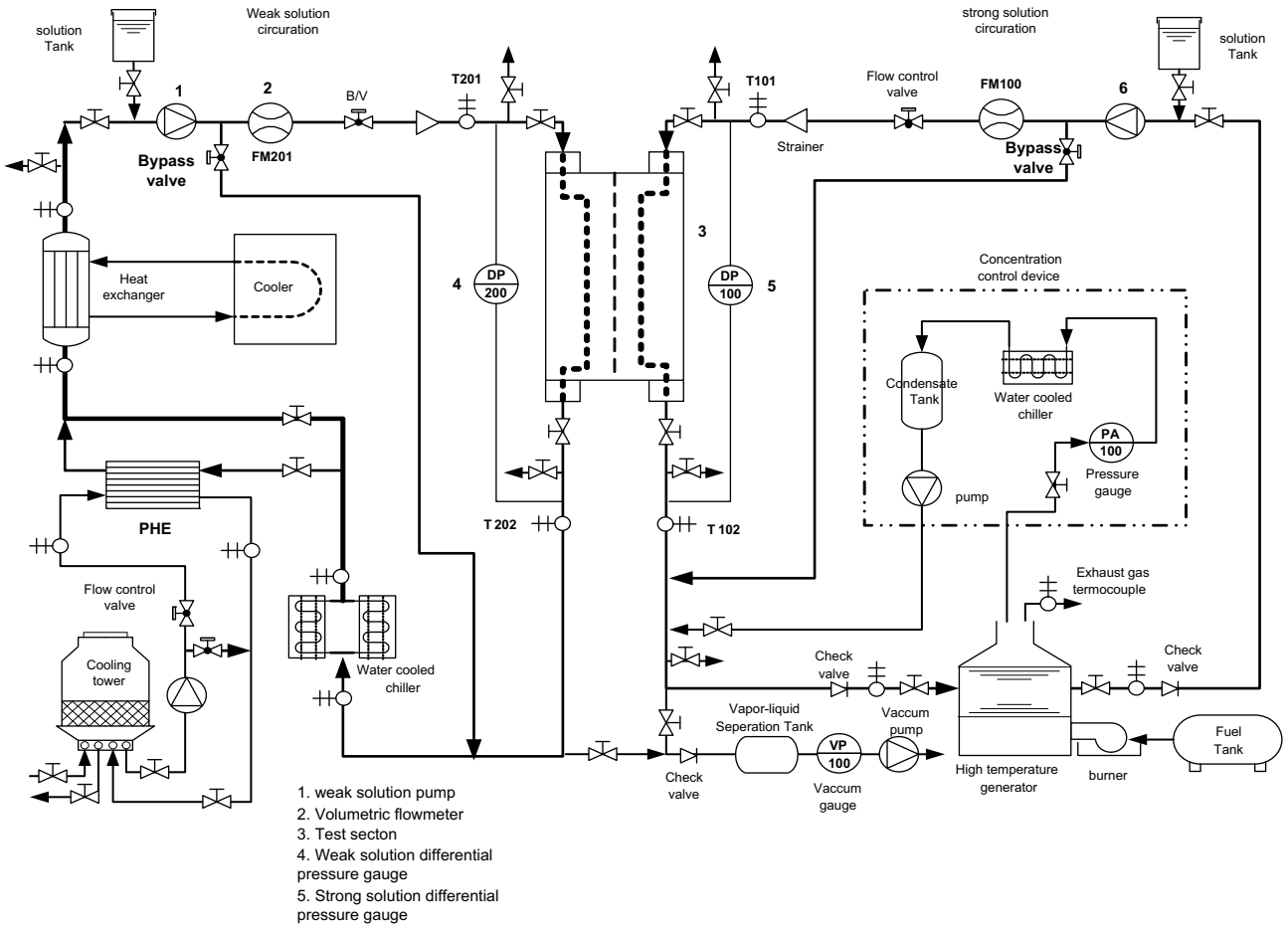


**Fig. 4 – Schematic diagram of experimental apparatus.**

## 3. Experimental setup and procedure

The experimental setup is shown in Fig. 4. The experimental apparatus consists of two solution circuits; a LiBr strong solution circuit and a weak solution circuit. The strong solution is heated by a high temperature generator. The refrigerant vapor generated in the high temperature generator is condensed in a water cooled condenser and joins the strong solution from the test section. The strong solution enters the test section at a higher temperature after passing through a magnetic pump and a flow meter. The strong solution releases heat to the weak solution, joins the condensed refrigerant and finally returns to the high temperature generator. There is a bypass line to control the mass flow rate of the strong solution.

As for the weak solution circuit, the weak solution from the test section joins the bypass line and enters the water cooled chiller to be cooled down. The weak solution releases more heat in a plate heat exchanger (PHE) which is connected to the cooling tower and its temperature is more precisely controlled by the final heat exchanger. Finally the weak solution enters the test section after passing through the bypass valve and the flow meter. The geometric details of the welded type plate heat exchanger are summarized in Table 2.

Calibrated RTDs are used to measure the temperatures of the solutions at the inlet/outlet of the test section with the measurement error of $\pm 0.1$ K. The solution flow rates of the test section are measured by volumetric flow-meters with the measurement error of $\pm 0.05\ kg\,s^{-1}$. The pressure drop of the solution flowing through the test section is measured with a differential pressure transducer with the experimental measurement error of $\pm 0.035$ kPa. The inlet temperature of the strong solution is controlled by heat source input in the high temperature generator and the inlet temperature of the weak solution is controlled by three heat exchangers with the cooling tower. The experimental conditions are summarized in Table 3. The thermo-physical properties of the $H_2O$/

**Table 2 – Geometric conditions of heat exchanger**

| Material | SPCC |
|---|---|
| Number of passes | 1 |
| Number of plates | 60 |
| Plate length (mm) | 1839 |
| Plate width (mm) | 294 |
| Plate thickness (mm) | 0.7 |
| Mean channel gap (mm) | 1.6 |
| Heat transfer area per plate ($m^2$) | 0.54 |

| Table 3 – Experimental conditions | |
|---|---|
| Concentration of LiBr | 51.8% (cold side)<br>59.38% (hot side) |
| Inlet solution Temperature of hot side | 420.0 K |
| Inlet solution Temperature of cold side | 362.0 K |
| Inlet solution flow rate of hot side | 1.08–1.8 kg s$^{-1}$ |
| Inlet solution flow rate of cold side | 1.2–2.0 kg s$^{-1}$ |

LiBr solution are calculated using the correlations derived from the data presented in DiGuilio et al. (1990) and Lee et al. (1990).

## 4. Data reduction

In this study, heat transfer rate and pressure drop are measured for the plate heat exchanger (PHE) with chevron embossing plates. The heat transfer performance is estimated by measuring the temperature difference of the strong and weak solution sides, and the pressure drop is measured directly by the pressure difference between the inlet and outlet of the test section. The flow characteristics are analyzed based on the Reynolds number defined as follows;

$$\mathrm{Re} = \frac{GD_h}{\mu} \tag{8}$$

where

$$G = \frac{\dot{m}}{A_c N_{FP}} \tag{9}$$

$$D_h = \frac{2bw}{(b+w)} \tag{10}$$

In Equations (8)–(10), $D_h$ and $N_{FP}$ are the hydraulic diameter and the number of flow passes for each solution side. Now the heat transfer rate is calculated by the follow equation;

$$Q = \dot{m}_c Cp_c \Delta T_c \tag{11}$$

where

$$\Delta T_c = T_{c,out} - T_{c,in} \tag{12}$$

The heat transfer equation is given by

$$Q = UA\Delta T_{lm} \tag{13}$$

where

$$\Delta T_{lm} = \frac{(T_{h,in} - T_{c,out}) - (T_{h,out} - T_{c,in})}{\ln\left[\frac{T_{h,in} - T_{c,out}}{T_{h,out} - T_{c,in}}\right]} \tag{14}$$

The pressure drops at hot (strong solution) and cold (weak solution) sides are calculated by Eq. (15) (Kakac and Liu, 1998). The first term in the right-hand side is the contribution of the friction loss inside the channels, where $G$ denotes the channel mass velocity (Eq. (9)), $f$ is the Fanning friction factor, $D_h$ is the hydraulic diameter of channel (Eq. (10)), $L$ is the effective plate length for the plate heat exchange. The second term in the right-hand side represents the pressure drop for port flow, where $G_p$ is the port mass velocity (Eq. (16)).

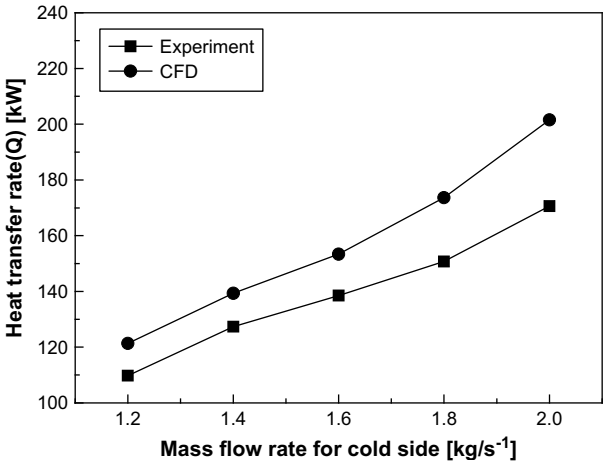


**Fig. 5 – Heat transfer rate versus mass flow rate for chevron embossing type.**

$$\Delta P = \left(\frac{2f(L+D_h)P_n G^2}{\rho_m D_h}\right) + 1.4\left(P_n \frac{G_p^2}{2\rho_m}\right) \tag{15}$$

$$G_p = \frac{4\dot{m}}{\pi D_p^2} \tag{16}$$

## 5. Results and discussion

Fig. 5 shows the heat transfer rate of the cold side solution versus the solution mass flow rate for the welded type plate heat exchanger with chevron embossing plates. The results show that the heat transfer rate increases with increasing the solution mass flow rate. Also the simulation results show the same trend as the experimental results but there is somewhat difference in the heat transfer value itself. This is

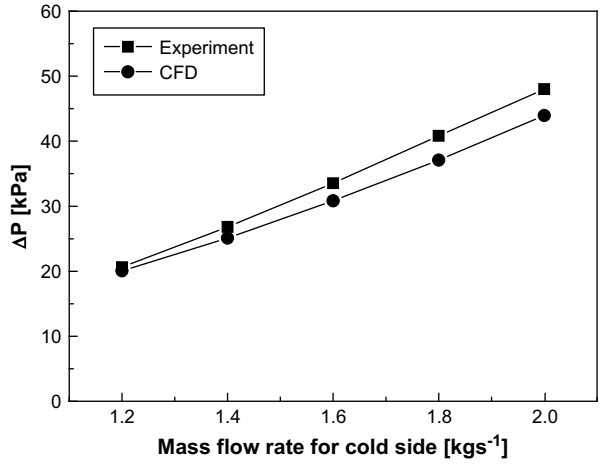


**Fig. 6 – Pressure drop versus mass flow rate for chevron embossing type.**

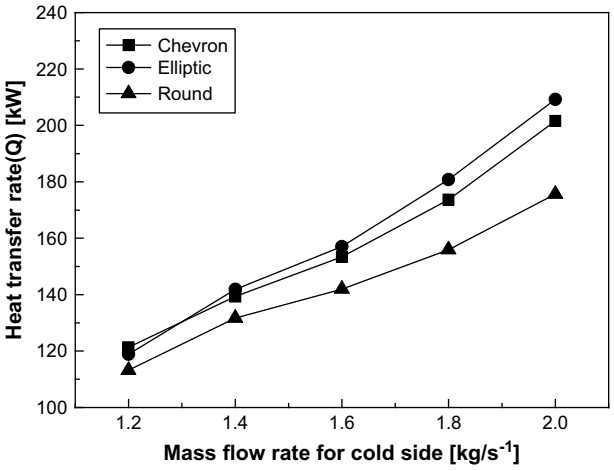


**Fig. 7 – Heat transfer rate versus mass flow rate for three different embossing plates.**

mainly due to heat loss to the surroundings during the experiment.

Fig. 6 shows the pressure drop versus the solution mass flow rate for the welded type plate heat exchanger with chevron embossing plates. It is found that the total pressure drop increases linearly with increasing the mass flow rate for the present range of the mass flow rate in both the simulation and the experimental results. The experimental results are 5–10% higher than the simulation results depending on the mass flow rate range, and the deviation becomes larger as the mass flow rate increases.

Fig. 7 shows comparisons of the chevron embossing type, the elliptic embossing type and the round embossing plates based on the solution heat transfer rate with respect to the mass flow rate. As shown in Fig. 5, the simulation results show the same trends as the experimental results. It is found that the solution heat transfer rate of the elliptic type is higher than those of the chevron and round embossing types. This means that the elliptic embossing type gives a better heat transfer performance than the elliptic embossing type, and the round embossing type under the same geometric and thermal conditions.

Fig. 8 shows the pressure drop versus the mass flow rate for chevron, elliptic and round embossing plate types. From this graph, it is found that the pressure drop of chevron embossing plate is much larger than those for other plates. This means that the chevron embossing plate heat exchanger needs more pumping power. Thus, by considering heat transfer and pressure drop characteristics, the elliptic embossing plate heat exchanger is considered the best candidate out of three types considered in the present study.

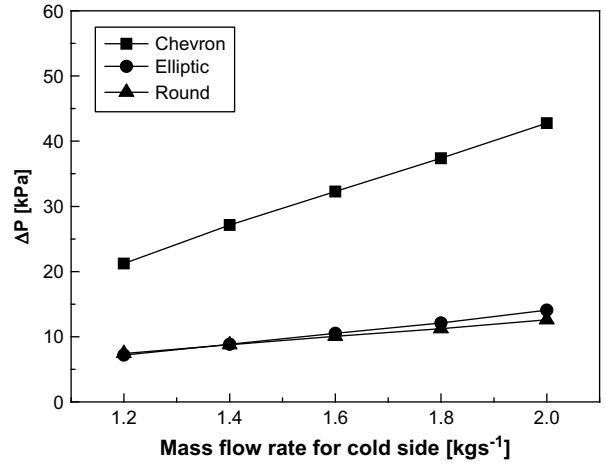


**Fig. 8 – Pressure drop versus mass flow rate for three different embossing plates.**

## 6. Conclusions

In this paper, a welded plate heat exchanger with three different embossing plates was proposed for solution heat exchanger application in absorption systems, and the characteristics of heat transfer and pressure drop of the welded type plate heat exchanger was studied. The following conclusions were drawn from the present study.

1) The simulation results show the same trends as the experimental results. The solution heat transfer rate increases with increasing the mass flow rate.
2) It is found that the elliptic embossing type gives better heat transfer performance than the chevron type plate and a lower pressure drop than the other plates under the same geometric and thermal conditions

The present results provide a guideline to apply the welded type plate heat exchanger with embossing plates for the solution heat exchanger of absorption systems.

## Acknowledgement

This work was supported by the Korea Energy Management Corporation Grant (2005-E-BD11-P-02-3-010-2007).

## REFERENCES

DiGuilio, R.M., Lee, R.J., Jeter, S.M., Teja, A.S., 1990. Properties of lithium bromide–water solution at high temperatures and concentrations – I thermal conductivity. ASHRAE Transactions 3380, 702–708. RP-527.

Galeazzo, Flazvio, C.C., Miyura, R.Y., Gut, Jorge, A.W., Tadini, C.C., 2006. Experimental and numerical heat transfer in a plate heat exchanger. Chemical Engineering Science 61, 7133–7138.

Hinze, J.O., 1975. Turbulence. McGraw-Hill Publishing Co., New York.

Kakac, S., Liu, H. (Eds.), 1998. Heat Exchangers: Selection, Rating and Thermal Design. CRC Press, New York, pp. 232–354.

Kim, H.J., Kim, J.H., Kim, S.S., Jeong, J.H., Kang, Y.T., 2005. Heat transfer and pressure drop characteristic of plate heat exchangers for absorption application. Proc. SAREK 2005 Winter Annual Conference, pp. 347–352.

Lee, R.J., DiGuilio, R.M., Jeter, S.M., Teja, A.S., 1990. Properties of lithium bromide–water solution at high temperatures and concentrations – II density and viscosity. ASHRAE Transactions 3381, 709–714. RP-527.

Phan, T.T., Lim, J.K., Moon, C.K., Yoon, J.I., 2000. Experiment of solution heat exchanger characteristics for absorption chiller and heater. Proc. SAREK 2000 Summer Annual Conference, pp. 688–693.

Ciofalo, M., Stasiek, J., Collins, M.W., 1996. Investigation of flow and heat transfer in corrugated passages-II, numerical simulations. International Journal of Heat and Mass Transfer 39 (1), 165–192.

de Vega, M., Almendros-Ibanez, J.A., Ruiz, G., 2006. Performance of a LiBr–water absorption chiller operating with plate heat exchangers. Energy Conversion and Management 47, 3393–3407.